AJNR

Evaluation of Dural Arteriovenous Fistulas with 4D Contrast-Enhanced MR Angiography at 3T

S. Nishimura, T. Hirai, A. Sasao, M. Kitajima, M. Morioka, Y. Kai, Y. Omori, T. Okuda, R. Murakami, H. Fukuoka, K. Awai, J.-I. Kuratsu and Y. Yamashita

AJNR Am J Neuroradiol 2010, 31 (1) 80-85
doi: https://doi.org/10.3174/ajnr.A1898
http://www.ajnr.org/content/31/1/80

ORIGINAL RESEARCH

Evaluation of Dural Arteriovenous Fistulas with 4D Contrast-Enhanced MR Angiography at 3T

S. Nishimura
T. Hirai
A. Sasao
M. Kitajima
M. Morioka
Y. Kai
Y. Omori
T. Okuda
R. Murakami
H. Fukuoka
K. Awai
J.-I. Kuratsu
Y. Yamashita

BACKGROUND AND PURPOSE: Four-dimensional contrast-enhanced MR angiography (4D-CE-MRA) at 3T may replace digital subtraction angiography (DSA) for certain diagnostic purposes in patients with intracranial dural arteriovenous fistula (DAVF). The aim of this study was to test the hypothesis that 4D-CE-MRA at 3T enables the same characterization of intracranial DAVFs as DSA.

MATERIALS AND METHODS: The study population consisted of 18 consecutive patients with intracranial DAVFs (11 women, 7 men; age range, 35–82 years; mean age, 64.8 years). They underwent 4D-CE-MRA at 3T and DSA. The 4D-CE-MRA series combined randomly segmented central *k*-space ordering, keyhole imaging, sensitivity encoding, and half-Fourier imaging. We obtained 30 dynamic scans every 1.9 seconds with a spatial resolution of 1 × 1 × 1.5 mm. Two independent readers reviewed the 4D-CE-MRA images for main arterial feeders, fistula site, and venous drainage. Interobserver and intermodality agreement was assessed by κ statistics.

RESULTS: At DSA, 8 fistulas were located at the transverse sigmoid sinus; 8, at the cavernous sinus; and 2, at the sinus adjacent to the foramen magnum. Interobserver agreement was fair for the main arterial feeders ($\kappa = 0.59$), excellent for the fistula site ($\kappa = 0.91$), and good for venous drainage ($\kappa = 0.86$). Intermodality agreement was moderate for the main arterial feeders ($\kappa = 0.68$) and excellent for the fistula site ($\kappa = 1.0$) and venous drainage ($\kappa = 1.0$).

CONCLUSIONS: The agreement between 4D-CE-MRA and DSA findings was good to excellent with respect to the fistula site and venous drainage.

Several studies have shown an association between the venous drainage patterns of intracranial dural arteriovenous fistula (DAVF) and the clinical presentation.[1,2] DAVFs draining retrogradely into cortical veins have a much higher incidence of hemorrhage or venous infarction.[3,4] The annual mortality rate for cortical venous reflux may be as high as 10.4%, whereas the annual risk for hemorrhage or nonhemorrhagic neurologic deficits during follow-up is 8.1% and 6.9%, respectively, resulting in an annual event rate of 15%.[4] Intra-arterial digital subtraction angiography (DSA) remains the criterion standard for the assessment of intracranial DAVF. Its inherent high spatial and temporal resolution facilitates the accurate analysis of the fistula site and the discernment of the feeding arteries and draining veins. However, DSA is invasive, exposes the patient to radiation, and requires the injection of iodinated contrast material. Therefore, a noninvasive method is needed for the accurate diagnosis of intracranial DAVFs, including their venous drainage patterns, and for pretreatment evaluation, treatment selection, and follow-up.

Several noninvasive techniques, including conventional MR imaging, 3D time-of-flight MR angiography (3D-TOF-MRA), and source images of 3D-TOF-MRA, have been used for the visualization of intracranial DAVF.[5-10] However, the clinical use of these techniques remains limited because of the lack of hemodynamic information and the possibility of misdiagnosis.[7-12]

Received March 21, 2009; accepted after revision May 30.

From the Departments of Diagnostic Radiology (S.N., T.H., A.S., M.K., T.O., H.F., K.A., Y.Y.), Neurosurgery (M.M., Y.O., J.-I.K.), and Radiation Oncology (R.M.), Graduate School of Medical Sciences, Kumamoto University, Kumamoto, Japan; and Department of Neurosurgery (Y.K.), Ryukyu University, Okinawa, Japan.

Please address correspondence to Toshinori Hirai, MD, Department of Diagnostic Radiology, Graduate School of Medical Sciences, Kumamoto University, 1–1-1 Honjo, Kumamoto, 860-8556 Japan; e-mail: t-hirai@kumamoto-u.ac.jp

DOI 10.3174/ajnr.A1898

Time-resolved contrast-enhanced MR angiography (MRA) at 1.5T has been applied to the diagnosis of intracranial DAVF.[13,14] It combines the T1 shortening effect of a gadolinium-based contrast agent, dynamic imaging, a digital subtraction technique, and parallel imaging techniques and yields high-temporal-resolution MRA.[13,14] Although the use of 3T for assessing intracranial and extracranial vascular malformations with time-resolved contrast-enhanced MRA has been described,[15,16] to our knowledge, systematic investigation of intracranial DAVF with this method at 3T has not been reported. MR imaging scanners at 3T provide a high signal-intensity–to-noise ratio. The temporal and spatial resolution can be further improved by applying intelligent *k*-space sampling techniques, which are provided by some vendors. One of the techniques is performed with segmented central *k*-space ordering (ie, contrast-enhanced robust-timing angiography [CENTRA]).[16-20]

The aim of our study was to compare prospectively the agreement between DSA and 4D contrast-enhanced MR angiography (4D-CE-MRA) in combination with keyhole acquisition and CENTRA *k*-space sampling techniques at 3T for the characterization of intracranial DAVF.

Materials and Methods

Study Population

Our study was approved by our institutional review board, and informed consent for imaging examinations was obtained from all patients or their relatives. Our study included 18 patients (11 women and 7 men ranging from 35 to 82 years of age; mean age, 64.8 years) with intracranial DAVFs who underwent 4D-CE-MRA between March 2007 and August 2008. Of these, 17 were initially diagnosed and 1 manifested a residual DAVF after embolization. All patients underwent intra-arterial DSA; the interval between DSA and MRA ranged from 3 to 22 days (mean, 9 days).

Table 1: Summary of DSA and 4D-CE-MRA findings in 18 DAVFs[a]

	4D-CE-MRA		Interobserver	4D-CE-MRA		Intermodality
	Reader 1	Reader 2	Agreement[b]	Consensus Reading	DSA	Agreement[c]
Fistula site						
CS	8	8	17 (94)	8	8	18 (100)
TS	8	8	[0.72–0.99]	8	8	[0.81–1.00]
FM	2	1		2	2	
Other sites	0	1		0	0	
Main feeders						
IMA-MMA	7	7	14 (78)	7	7	16 (89)
APA	7	5	[0.52–0.94]	5	4	[0.65–0.98]
OA	3	5		6	7	
ICA	0	0		0	0	
Other feeders	1	1		0	0	
Venous drainage						
Type 1[d]	14	13	16 (89)	13	13	18 (100)
Type 2[e]	3	4	[0.65–0.98]	4	4	[0.81–1.00]
Type 3[f]	1	1		1	1	

Note:—4D-CE-MRA indicates 4D contrast-enhanced MR angiography; DSA, digital subtraction angiography; DAVF, dural arteriovenous fistula; CS, cavernous sinus; TS, transverse-sigmoid sinus; FM, sinus adjacent to the foramen magnum; IMA-MMA, internal maxillary artery and/or middle meningeal artery; APA, ascending pharyngeal artery; OA, occipital artery; ICA, internal carotid artery; CI, confidence interval.
[a] Data are number of DAVFs. Data in parentheses are the percentage of concordance, and data in brackets are exact CIs.
[b] Agreement of 4D-CE-MRA between reader 1 and reader 2.
[c] Agreement between the consensus reading at 4D CE-MRA of reader 1 and reader 2 and DSA.
[d] Venous drainage directly into the dural venous sinus.
[e] Venous drainage into the dural venous sinus with cortical venous reflux.
[f] Venous drainage directly into the subarachnoid veins (cortical venous reflux only).

Table 2: Interobserver and intermodality agreement for DAVF characterization[a]

	Main Arterial Supply	Fistula Site	Venous Drainage
Interobserver agreement[b]	0.59 (0.29–0.90)	0.91 (0.73–1.00)	0.86 (0.60–1.00)
Intermodality agreement[c]	0.68 (0.40–0.96)	1.00 (1.00–1.00)	1.00 (1.00–1.00)

[a] Data are κ statistics, with 95% CIs in parentheses.
[b] Agreement of 4D-CE-MRA between reader 1 and reader 2.
[c] Agreement between the consensus reading at 4D-CE-MRA of reader 1 and reader 2 and DSA.

DSA showed that of the 18 DAVFs, 8 were located at the transverse-sigmoid sinus (TS); 8, at the cavernous sinus (CS); and 2, at the sinus adjacent to the foramen magnum (FM) (the hypoglossal canal). The primary presenting symptoms were headache in 10 patients, double vision in 5, seizures in 2, and tinnitus in 1 patient.

DSA Technique

After catheterization of the internal and external carotid and the vertebral arteries via a femoral artery approach, diagnostic biplanar intra-arterial DSA (Allura Xper FD; Philips Medical Systems, Best, the Netherlands) was performed by a trained neuroradiologist and a neurosurgeon. Images were obtained with a 1024 × 1024 matrix and an FOV of 17 cm. Temporal resolution of the images was 3 frames per second. For each projection, a 6- to 10-mL bolus of undiluted iodinated contrast material with an iodine concentration of 300 mg/mL (isopamidol, Iopamiron 300; Bayer-Schering, Berlin, Germany) was manually injected.

MR Imaging

4D-CE-MRA was performed on a 3T MR imaging system (Achieva; Philips Medical Systems) by using a commercially available 8-channel head coil. The MR imaging unit was equipped with a gradient system that allowed a maximal achievable gradient amplitude of 40 mT/m, a rise time of 0.2 ms, and a slew rate of 200 T/m/s.

The patients were positioned with a 20-gauge intravenous catheter inserted into the antecubital vein. The intravenous injection of 0.2-mL gadopentetate dimeglumine (Magnevist; Bayer-Schering) per kilogram of body weight (flow rate, 3 mL/s) was followed by a 30-mL saline flush delivered with an automated power injector. 4D-CE-MRA was started after the injection of the contrast agent. The acquisition parameters for 4D-CE-MRA were the following: TR/TE, 2.9 ms/1.4 ms; flip angle, 20°; image matrix, 256 × 256; FOV, 256 mm covering the entire head.

A combination of keyhole acquisition with a segmented central *k*-space ordering (CENTRA) technique was used to improve temporal resolution at CE-MRA at a constant spatial resolution.[17,18] We acquired 120 thin sagittal partitions of 2 mm with a 1-mm overlap between sections by using a sensitivity encoding (SENSE) factor of 2 in the section-selection direction and of 4 in the phase-encoding direction and a keyhole diameter of 15%; this yielded a voxel size of 1.0 × 1.0 × 1.5 mm (1.5 mm^3) with zero-filling. In total, 24 dynamic volumes were acquired with an average keyhole imaging duration of 1.9 s/volume, followed by dynamic reference imaging with a duration of 3.9 seconds. The total acquisition time for the 4D-CE-MRA sequence was 50 seconds. Time-resolved MRA yielded a total acceleration factor of 88.8 (6.66 [15% keyhole] × 8 [SENSE]) / 0.6 [half-scan factor]) compared with standard CE-MRA without such techniques. Image processing included mask subtraction to suppress the background signal intensity of stationary tissue. Images were displayed with a reconstructed isotropic image matrix of 1 × 1 × 1 mm. In addition, routine MR imaging included pre- and postcontrast T1-weighted spin-echo and T2-weighted fast spin-echo sequences.

Image Analysis

Independent readers (T.H. or Y.O. with 20 and 10 years of experience in neuroangiography, respectively) qualitatively evaluated the entire series of DSA images on a PACS workstation. They reviewed evaluations that did not agree to reach a consensus. Two other readers (T.O. and M.K. with 21 and 18 years of experience in neuroradiologic MR imaging, respectively) independently evaluated the 4D-CE-MRA data at a PACS workstation; they were blinded to the clinical and DSA results. The 3D data were displayed with all regions visible. The soft-

ware allowed the enlargement of regions of special interest in any given spatial orientation.

4D-CE-MRA and conventional DSA data were assessed for the fistula site, the main arterial feeders, and the venous drainage of the underlying DAVF. Main arterial feeders were defined as branches deriving from the internal maxillary and/or middle meningeal artery (IMA-MMA), the ascending pharyngeal artery (APA), the occipital artery (OA), the internal carotid artery, or other arteries. DAVFs were classified with respect to the fistula site as fistulas at the CS, the TS, the sinuses adjacent to the FM, and other sites. According to the classification of Borden et al,[2] DAVF drainage was recorded as type 1, drainage directly into the dural venous sinus; type 2, drainage into the dural venous sinus with cortical venous reflux; and type 3, drainage directly into subarachnoid veins (cortical venous reflux only). The 2 readers re-evaluated assessments that did not agree until a consensus was reached.

Statistical Analysis

The levels of interobserver agreement (between readers 1 and 2 for DSA and 4D-CE-MRA) and intermodality agreement (between consensus readings of 4D-CE-MRA and DSA images) with respect to the main arterial feeders, fistula site, and venous drainage were determined by calculating the κ coefficient ($\kappa < 0.20$ = poor, $\kappa = 0.21$–0.40, fair; $\kappa = 0.41$–0.60, moderate; $\kappa = 0.61$–0.80, good; $\kappa = 0.81$–0.90, very good; and $\kappa > 0.90$, excellent agreement). In addition, we recorded the exact number and percentage of times when results from the 2 readers and the 2 modalities were in exact agreement, including exact and 95% confidence intervals (CIs). A statistical package, MedCalc for Windows (MedCalc Software, Mariakerke, Belgium), was used for all analyses.

Results

In the qualitative evaluation of DSA, the interobserver agreement was excellent for all items ($\kappa = 1.0$; 95% CI, 1.0–1.0). Table 1 is a summary of the DSA and 4D-CE-MRA findings on the 18 DAVFs.

On DSA images, 7 DAVFs were primarily supplied by the IMA-MMA, 7 by the OA, and 4 by the APA. In 16 of 18 studies (89%), the 4D-CE-MRA (consensus reading) and DSA findings of the 2 readers coincided with respect to the main arterial feeders to the DAVF (exact CI, 0.65–0.98). Intermodality agreement (consensus reading of 4D-CE-MRA versus DSA) was moderate ($\kappa = 0.68$; 95% CI, 0.40–0.96) (Table 2). In the analysis of the main arterial feeders to the DAVF, the 2 readers reviewing 4D-CE-MRA images agreed in 14 of 18 studies (78%; exact CI, 0.52–0.93); the interobserver agreement was recorded as fair ($\kappa = 0.59$; 95% CI, 0.29–0.90) (Figs 1 and 2).

On DSA images, 8 fistulas were located at the TS, 8 at the CS, and 2 at the FM. 4D-CE-MRA (consensus reading) and DSA findings were in agreement with respect to the fistula site in all 18 patients (exact CI, 0.81–1.00). Intermodality agreement between DSA and 4D-CE-MRA was excellent ($\kappa = 1.0$; 95% CI, 1.0–1.0). Independently, the readers agreed on the fistula site in 17 (94%) of the 18 patients (exact CI, 0.72–0.99); agreement was excellent ($\kappa = 0.91$; 95% CI, 0.73–1.0) (Table 2 and Figs 1 and 2).

On DSA, venous drainage was type 1 in 13 patients (72%), type 2 in 4 (22%), and type 3 in 1 (6%). Intermodality agreement for venous drainage was excellent ($\kappa = 1.0$; 95% CI, 1.0–1.0). On 4D-CE-MRA images, the readers agreed on the venous drainage pattern in 16 of 18 patients (89%) (exact CI, 0.65–0.98); interobserver agreement was good ($\kappa = 0.86$; CI, 0.6–1.0) (Table 2 and Figs 1 and 2).

Discussion

Our study showed that 4D-CE-MRA on a 3T scanner with parallel imaging combined with keyhole acquisition and CENTRA *k*-space sampling was a reliable diagnostic tool for the characterization of intracranial DAVF, especially with respect to the fistula site and the route of venous drainage. We attribute the excellent interobserver and intermodality agreement to the relatively high temporal and spatial resolution. The 4D-CE-MRA sequence we used was based on a combination of SENSE, keyhole acquisition, half-scan, and CENTRA *k*-space sampling techniques.[16-20] These techniques yielded a total acceleration factor of 88.8 compared with the standard CE-MRA technique. This acceleration allows data acquisition of the MR images with a spatial resolution of $1 \times 1 \times 1.5$ mm and a temporal resolution of 1.9 s/volume. In our study, the spatial and temporal resolutions of DSA were 0.17×0.17 mm and 3 frames per second, respectively. Although the resolution of 4D-CE-MRA was inferior to that of DSA, the 4D-CE-MRA must have had sufficient resolution to identify the spatial location of the vasculature and differentiate the early arterial, arterial, parenchymal, and venous phases.

In the assessment of the main arterial feeders, interobserver and intermodality agreement was fair and moderate, respectively. Compared with the voxel size of 4D-CE-MRA images, the diameter of arterial DAVF feeders is often small, and the spatial resolution on these images may not be high enough to depict small feeders. Further technical advances are required to improve the visualization of arterial feeders.

On the basis of our study, 4D-CE-MRA would replace DSA in the primary diagnosis regarding the presence or absence of intracranial DAVF and in the follow-up study. Because 4D-CE-MRA cannot yet provide complete characterization of the DAVF, DSA would remain as a definitive tool for determining the treatment decision and strategy. Studies on larger populations are necessary to clarify the role of 4D-CE-MRA in patients with intracranial DAVF.

There are some limitations to our study. First, we did not compare 4D-CE-MRA and conventional nonenhanced MRA findings. Conventional MRA may provide additional information, especially about the arterial supply of DAVF. Second, because our data were obtained in a single-center study with a small study population, we cannot draw conclusions with respect to the equivalence of 4D-CE-MRA and DSA. Third, our study did not address the actual number of vessels supplying and draining individual DAVFs; this might have affected our results.

In conclusion, the good-to-excellent agreement between 4D-CE-MRA and DSA findings suggests that 4D-CE-MRA is a reliable tool for the characterization of intracranial DAVF with respect to the fistula site and venous drainage. 4D-CE-MRA could be used in the primary diagnosis regarding the presence or absence of intracranial DAVF and in the follow-up study. Further technical advances are required to improve the visualization of arterial feeders.

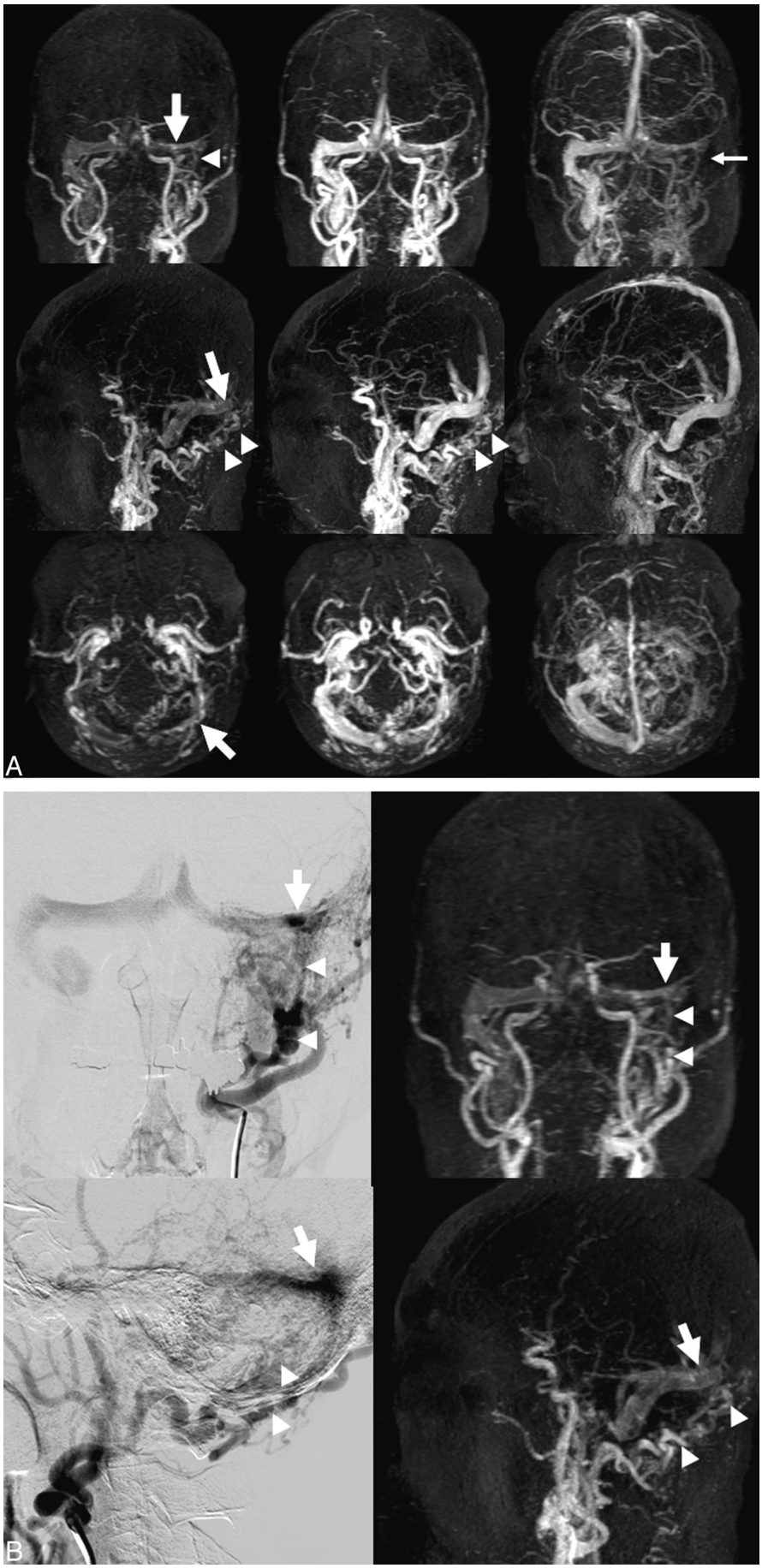

Fig 1. *A,* Anteroposterior (top row), lateral (second row), and axial (bottom row) projections of maximum-intensity 4D-CE-MRA images (2.9/1.4, 20° flip angle) reconstructed in a 65-year-old man with DAVF at the left transverse sinus. There is an early depiction of the left transverse and the right transverse-to-sigmoid sinuses at the early arterial (left) to the arterial phase (middle). The fistula site (*arrow*) appears to be the left transverse sinus, and the DAVF is mainly supplied by branches from the occipital artery (*arrowheads*). Venous drainage is from the left transverse to the right transverse to the sigmoid sinus. The left sigmoid sinus is not visualized at the venous phase (*small arrow*). In this DAVF, both readers judged that the occipital artery was the main arterial feeder, the left transverse sinus was the fistula site, and venous drainage was type 1. *B,* Anteroposterior (upper) and lateral (lower) projections of digital subtraction angiography (DSA) (left) and 4D CE-MRA (right) during the arterial phase in the patient in *A*. DSA shows an arteriovenous shunt (*arrow*) at the left transverse sinus, which is supplied by branches from the occipital artery (*arrowheads*). 4D-CE-MRA also depicts the main arterial feeders (*arrowheads*), the fistula site (*arrow*), and the venous drainage route.

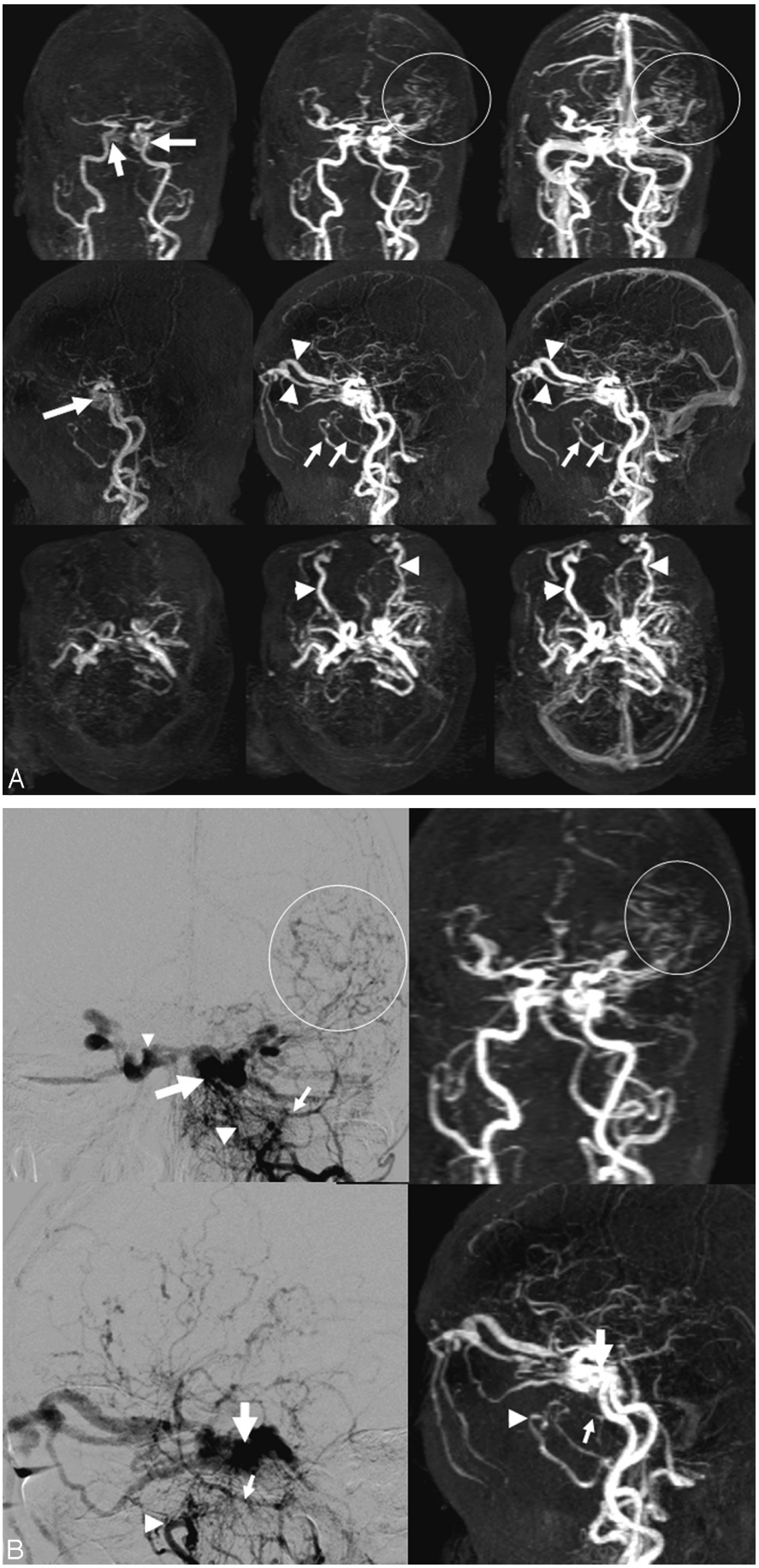

Fig 2. *A,* Anteroposterior (top row), lateral (second row), and axial (bottom row) projections of maximum-intensity 4D-CE-MRA images (2.9/1.4, 20° flip angle) of a 71-year-old woman with DAVF at the left cavernous sinus. There is an early depiction of the bilateral cavernous sinuses (*arrows*) at the early arterial phase (left). The bilateral superior ophthalmic veins (*arrowheads*) are dilated during the arterial (middle) and late arterial phase (right). The bilateral internal maxillary arteries are well visualized (*small arrows*). Retrograde cortical venous drainage is via the left cerebral cortical veins (*circle*). Both readers judged that this DAVF was primarily fed by the internal maxillary artery, that the cavernous sinus was the fistula site, and that venous drainage was type 2. *B,* Anteroposterior (upper) and lateral (lower) projections of DSA (left) and 4D-CE-MRA (right) images in the arterial phase in the patient in *A*. DSA shows an arteriovenous shunt (*arrow*) at the left cavernous sinus. It is supplied by branches from the left internal maxillary (*arrowhead*) and middle meningeal arteries (*small arrow*). The right cavernous sinus (*small arrowhead*) is depicted via the intercavernous sinus. Retrograde cortical venous drainage is via the left cerebral cortical veins (*circle*). 4D-CE-MRA also depicts the main arterial feeders (*arrowhead, small arrow*), the fistula site (*arrow*), and the venous drainage pattern (*circle*).

References

1. Cognard C, Gobin YP, Pierot L, et al. **Cerebral dural arteriovenous fistulas: clinical and angiographic correlation with a revised classification of venous drainage.** *Radiology* 1995;194:671–80
2. Borden JA, Wu JK, Shucart WA. **A proposed classification for spinal and cranial dural arteriovenous fistulous malformations and implications for treatment.** *J Neurosurg* 1995;82:166–79
3. Duffau H, Lopes M, Janosevic V, et al. **Early rebleeding from intracranial dural arteriovenous fistulas: report of 20 cases and review of the literature.** *J Neurosurg* 1999;90:78–84
4. van Dijk JM, terBrugge KG, Willinsky RA, et al. **Clinical course of cranial dural arteriovenous fistulas with long-term persistent cortical venous reflux.** *Stroke* 2002;33:1233–36
5. DeMarco K, Dillon WP, Halbach VV, et al. **Dural arteriovenous fistula: evaluation with MR imaging.** *Radiology* 1990;175:193–99
6. Chen JC, Tsuruda JS, Halbach VV. **Suspected dural arteriovenous fistula: results with screening MR angiography in seven patients.** *Radiology* 1992;183:265–71
7. Hirai T, Korogi Y, Hamatake S, et al. **Three-dimensional FISP imaging in the evaluation of carotid cavernous fistula: comparison with contrast-enhanced CT and spin-echo MR.** *AJNR Am J Neuroradiol* 1998;19:253–59
8. Kwon BJ, Han MH, Kang HS, et al. **MR imaging findings of intracranial dural arteriovenous fistulas: relations with venous drainage patterns.** *AJNR Am J Neuroradiol* 2005;26:2500–07
9. Meckel S, Maier M, Ruiz DS, et al. **MR angiography of dural arteriovenous fistulas: diagnosis and follow-up after treatment using a time-resolved 3D contrast-enhanced technique.** *AJNR Am J Neuroradiol* 2007;28:877–84
10. Ouanounou S, Tomsick TA, Heitsman C, et al. **Cavernous sinus and inferior petrosal sinus flow signal on three-dimensional time-of-flight MR angiography.** *AJNR Am J Neuroradiol* 1999;20:1476–81
11. Paksoy Y, Genc BO, Genc E. **Retrograde flow in the left inferior petrosal sinus and blood steal of the cavernous sinus associated with central vein stenosis: MR angiographic findings.** *AJNR Am J Neuroradiol* 2003;24:1364–68
12. Sakamoto M, Taoka T, Iwasaki S, et al. **Paradoxical parasellar high signals resembling shunt diseases on routine 3D time-of-flight MR angiography of the brain: mechanism for the signals and differential diagnosis from shunt diseases.** *Magn Reson Imaging* 2004;22:1289–93
13. Noguchi K, Melhem ER, Kanazawa T, et al. **Intracranial dural arteriovenous fistulas: evaluation with combined 3D time-of-flight MR angiography and MR digital subtraction angiography.** *AJR Am J Roentgenol* 2004;182:183–90
14. Akiba H, Tamakawa M, Hyodoh H, et al. **Assessment of dural arteriovenous fistulas of the cavernous sinuses on 3D dynamic MR angiography.** *AJNR Am J Neuroradiol* 2008;29:1652–57
15. Ziyeh S, Strecker R, Berlis A, et al. **Dynamic 3D MR angiography of intra- and extracranial vascular malformations at 3T: a technical note.** *AJNR Am J Neuroradiol* 2005;26:630–34
16. Hadizadeh DR, von Falkenhausen M, Gieseke J. **Cerebral arteriovenous malformation: Spetzler-Martin classification at subsecond-temporal-resolution four-dimensional MR angiography compared with that at DSA**. *Radiology* 2008;246:205–13. Epub 2007 Oct 19
17. van Vaals JJ, Brummer ME, Dixon WT, et al. **"Keyhole" method for accelerating imaging of contrast agent uptake.** *J Magn Reson Imaging* 1993;3:671–75
18. Farb RI, McGregor C, Kim JK, et al. **Intracranial arteriovenous malformations: real-time auto-triggered elliptic centric-ordered 3D gadolinium-enhanced MR angiography—initial assessment.** *Radiology* 2001;220:244–51
19. Willinek WA, Gieseke J, Conrad R, et al. **Randomly segmented central k-space ordering in high-spatial-resolution contrast-enhanced MR angiography of the supraaortic arteries: initial experience.** *Radiology* 2002;225:583–88
20. Taschner CA, Gieseke J, Le Thuc V, et al. **Intracranial arteriovenous malformation: time-resolved contrast-enhanced MR angiography with combination of parallel imaging, keyhole acquisition, and k-space sampling techniques at 1.5 T.** *Radiology* 2008;246:871–79